

EXPERIMENTAL CHARACTERIZATION OF THE MECHANICAL PROPERTIES OF 3D PRINTED BÉZIER-BASED LATTICE BEAMS

A. Álvarez-Trejo*, E. Cuan-Urquizo*†, and A. Roman-Flores*†

* Tecnológico de Monterrey, School of Science and Engineering, Av. Eugenio Garza Sada 2501
Sur, Monterrey 64849, Mexico

† Tecnológico de Monterrey, Institute of Advanced Materials for Sustainable Manufacturing,
Av. Eugenio Garza Sada 2501 Sur, Monterrey 64849, Mexico

Abstract

Architected materials are widely used in additive manufacturing to reduce weight. The controlled arrangement of material allows to tailor their mechanical properties by tuning their geometrical parameters. A parametrization based on cubic Bézier curves is employed here to generate lattice beams by changing the position of a free control point. Two topologies with the same volume fraction and base curve for the lattice constituent elements at different positions are studied and compared. Lattice beams are manufactured via Fused Filament Fabrication of polylactic acid. The effective stiffness and yield stress of these lattice beams is analyzed experimentally using three-point bending tests. Adjusting the control point location leads to tailoring the effective mechanical properties of the lattice beams. This methodology leads to the synthesis of architected topologies with customized mechanical properties.

Introduction

Cellular materials, also known as lattices or metamaterials, are controlled arrangements of material filling a defined volume. Some advantages of using cellular materials are minimal use of material, energy absorption, and high flexibility [1]. Cellular materials are used to manufacture lightweight parts, creating sandwich structures and applications for the transport sector [2, 3]. Given that the lattice-conforming elements are significantly smaller than the macro dimensions of the filled volume, cellular materials can be considered as homogeneous and described in terms of effective properties, which can be obtained experimentally as the properties of a solid material would [4]. These effective properties are a function of the lattice topology and volume fraction [5], i.e., the percentage of volume occupied by solid material. Then, the effective mechanical properties of a lattice, such as its stiffness, could be tailored by modifying parameters defining its topology. Complex parametric curves such as NURBS [6], B-splines [7, 8], or Bézier curves [9] have been used to define the topology of lattices, where changing the position of the curve-defining control points modifies the effective mechanical properties of these lattices. An increased curvature in the lattice topology has shown to increase the flexibility of the structures [10].

A controlled arrangement of material can be used to build beam-type structures, and their effective properties compared to those of equivalent homogeneous solid structures. The mechanical properties of these lattice beams have been studied in static loading conditions, such as in the study by Meng et al. [11], who analyzed the bending of sandwich panels with a three-dimensional kagome lattice core. Similarly, Wang et al. [12] created lattice beams and obtained their flexural rigidity in two bending planes. This mechanical characterization can also be done computationally, such as in the work by Álvarez-Trejo et al. [13], who studied the influence of

shear on the in-plane deflection of hexagonal and re-entrant lattice beams, via numerical models. Lattice beams conformed of structured materials have various applications, such as the one developed by Eremeyev et al. [14], who proposed analytical and numerical models for the enriched buckling of a pantographic beam arrangement. Additionally, Gu et al. [15] used a porous core on a sandwich panel to induce a twist and increase the aerodynamic efficiency of a rotor blade.

Few works focus on the experimental characterization of the mechanical properties of lattice beams; moreover, cellular topologies based on parametric curves have not been used to conform lattice beams. In this work, we focus on the out-of-plane flexural properties of Bézier-based lattice arrangements.

Methodology

Design and manufacturing of Bézier-based lattice beam samples

Here, two sets of Bézier-based lattices were generated from a base cubic Bézier curved segment. The definition of this curve is based on the methodology proposed in [9], but now controlling the position of the free control point by means of two independent variables: the distance r from the origin and the angle β describing its position. See Figure 1a, where the cubic curve has fixed starting and ending control points (P_0 and P_3). The distance between these points is λ , and they are placed in the horizontal axis so that the midpoint of the cubic Bézier curve is coincident with $x = \lambda/2$. The position of a free control point P_1 is then defined by the distance r and the angle β , as shown in Figure 1a. Control point P_2 acts as a double mirror of P_1 so that the cubic Bézier curve is symmetric. All Bézier curved segments were thickened to a total thickness t and arranged into two different topologies by rotating, flipping, and repeating the base curve. The two topologies studied here are labeled as *single curve* and *double curve*, shown in Figure 1b and Figure 1c, respectively.

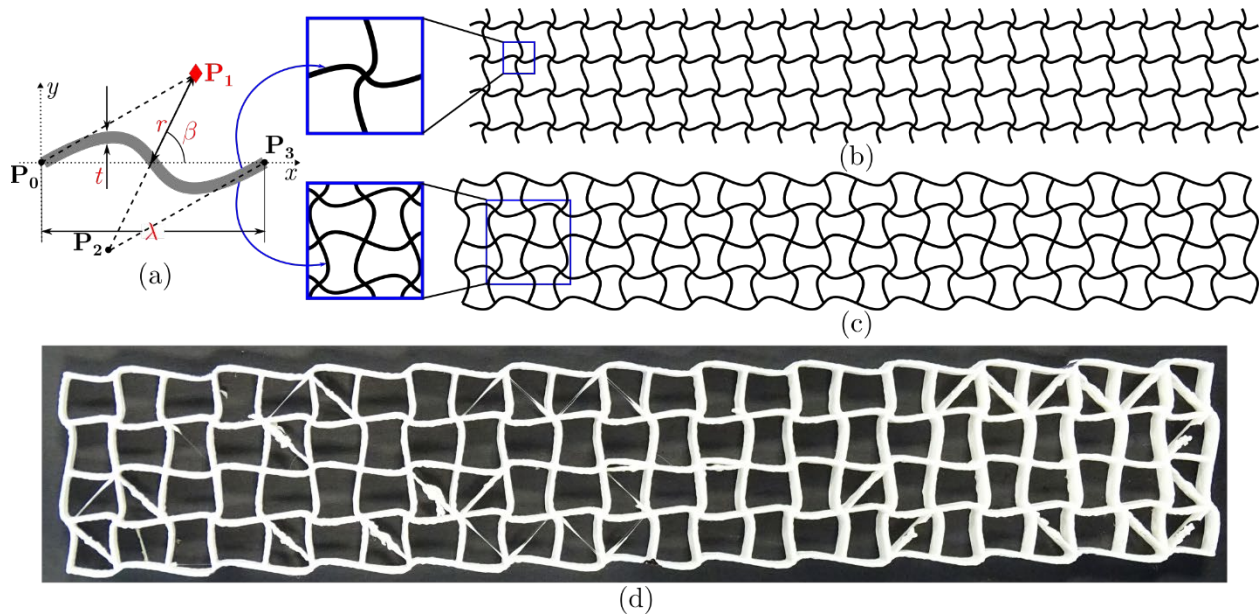


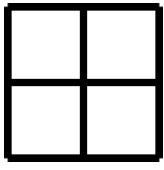
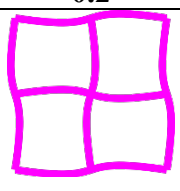
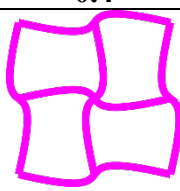
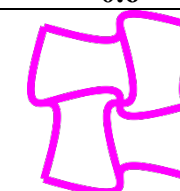
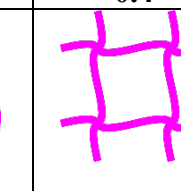
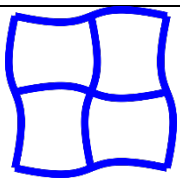
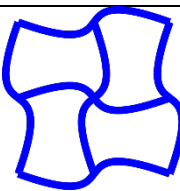
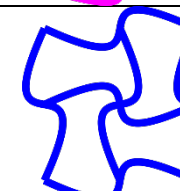
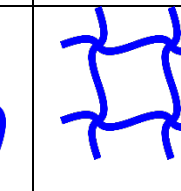
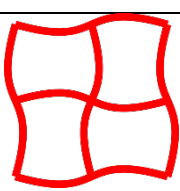
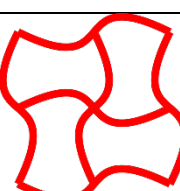
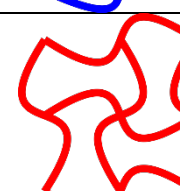
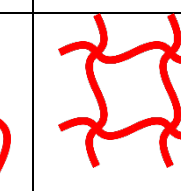
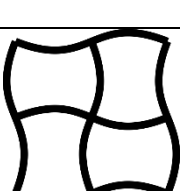
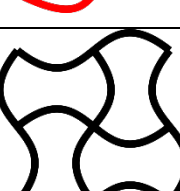
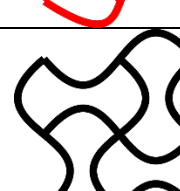
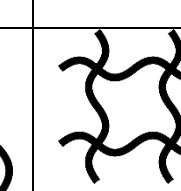
Figure 1. Lattice beam generation: (a) Base Bézier segment and defining geometric parameters. Two topologies are generated: (b) single curve and (c) double curve. An example of a 3D-printed sample is shown in (d).

For the experimental design, a set of samples of the double curve topology (see Figure 1c) was manufactured, using four values of β : 30° , 45° , 60° , and 90° . For this first set, the distance r between the origin and control point \mathbf{P}_1 took the values $r = 2$ mm, $r = 4$ mm, and $r = 6$ mm. Finally, the unit cell length was set constant at $\lambda = 10$ mm. Samples of each topology are depicted in Table 1; $r = 0$ produces the square lattice, which is considered for comparison purposes for all values of β .

A second set of samples was generated for the single curve topology (Figure 1b). In this case, the value of the angle β was fixed at $\beta = 90^\circ$ and the unit cell length was now set to $\lambda = 5$ mm, in order to match the volume fraction of the double curve topology. The distance r was set to $r = 2$ mm, so that $r/\lambda = 0.4$ as in one of the cases of the double curve topology.

In both cases, the thickness of the curved elements was kept constant at $t = 0.5$ mm. This thickness was proposed based on the printer nozzle diameter, so that each cubic Bézier curve was printed in a single step. All CAD files were generated with SOLIDWORKS® 2021, using global variables and configurations for parameter variation inside a single CAD file. The generated geometries were then converted to independent STL files for 3D printing.

Table 1. Representative views of each fabricated topology.

		r/λ				
		Double curve				Single curve
		0	0.2	0.4	0.6	0.4
β	30°					
	45°					
	60°					
	90°					

Considering all the combinations in Table 1, lattice beams were generated with external dimensions, as length $l = 120$ mm, width $w = 20$ mm, and depth $d = 4$ mm. Samples were fabricated via Fused Filament Fabrication (FFF), using the Ultimaker® 2+ printer and white Ultimaker®

polylactic acid (PLA). Ultimaker® Cura v4.10 was used to prepare the samples for printing. STL files were sliced with a layer height of 0.15 mm and considering a nozzle diameter of 0.4 mm. Samples were placed flat in the building plate, so that the direction of the depth d was the same as the building direction, which allowed to print without the need for supports or build plate adhesion. Samples were placed at the build plate in the same orientation, with nine lattice beams per printing job. The printing speed was kept constant at 50 mm/s and print cooling was enabled. Three replicates of each design were printed.

Mechanical testing of lattice beam samples

According to Euler-Bernoulli beam theory, the maximum deflection δ of a simply supported beam loaded at the midpoint is $\delta = FL^3/(48EI)$, where F is the applied load, L the effective length of the beam, E the Young's modulus, and I the second moment of area [16]. Given that the simply supported beam is made of a structured material, we assume that it behaves as a solid material with equivalent effective elastic properties. The product EI of the Young's modulus and second moment of area is then replaced by the effective bending stiffness $\langle EI \rangle$. This allows incorporating the effect of the topology and external geometry in the load-deflection behavior, since variable curvature in the lattice beams affects the shape of the external geometry.

Lattice beam samples were tested in three-point bending at $L = 100$ mm, placing each sample in a pair of supports and aligning to apply the load at the center of the beam. For the mechanical tests, a Perten Instruments® TTV6700 texture analyzer with a 50-kilogram load cell was used. The machine was setup in displacement-control mode, with a test speed of 0.5 mm/s and a maximum displacement of 12 mm. An example of the mechanical test setup and the resulting load-displacement curve can be found on the left side of Figure 2.

For each of the load-displacement curves obtained from the texture analyzer, two points were extracted, as shown on the right side of Figure 2. In first place, the displacement δ corresponding to $F = 0.5$ N was extracted to calculate the bending stiffness of the lattice beam. This value was selected because it is within the linear elastic range for all the topologies tested. In second place, the peak force F_p was extracted to calculate the yield stress $\langle \sigma \rangle$ of the lattice beam, which can be calculated as $\langle \sigma \rangle = 3F_p L / (2d^2 w)$. Here, d is the depth of the beam in the load direction, while w is the width out of the loading plane.

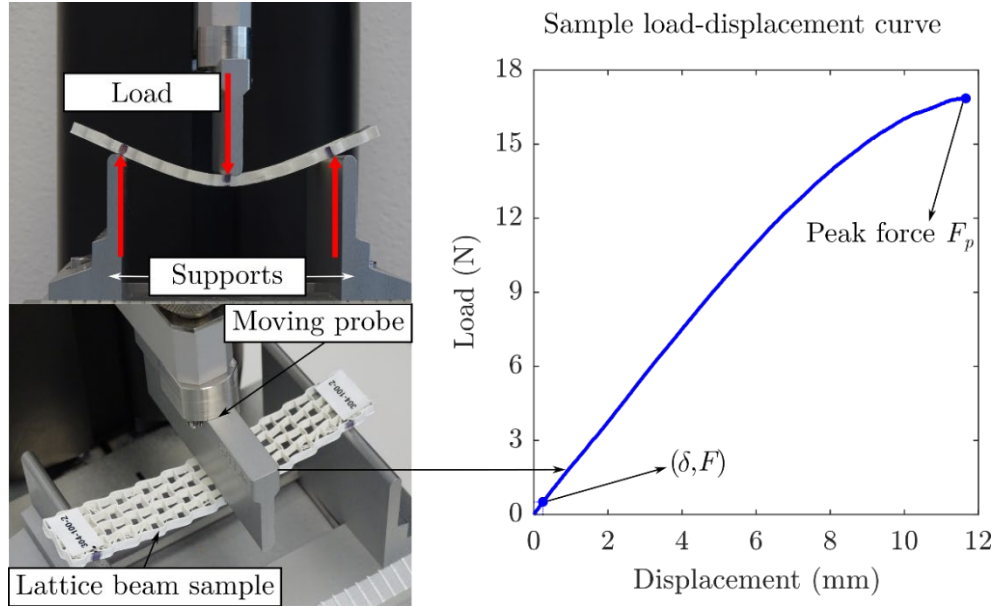


Figure 2. Left: Setup of the mechanical test. Right: Sample stress-strain curve corresponding to that sample. The displacement δ corresponding to $F = 0.5$ N, which is used for effective stiffness calculation, is marked in the plot, along with the peak force F_p used to calculate yield stress.

Results

Bending stiffness results of the mechanical testing of the double curve topology are presented as a function of r/λ in Figure 3 (left side). Values are obtained from the simply supported beam equation, as $\langle EI \rangle = FL^3/(48\delta)$, where F and δ are obtained from each stress-strain curve. Mean values from the three replicates were calculated and plotted with ± 1 standard deviation error bars. Increasing r/λ results in a lower bending stiffness: for $r/\lambda = 0.6$ and $\beta = 30^\circ$, the bending stiffness of the lattice beam is 72.61% smaller than for the square topology. Note that smaller values of β result in larger values of bending stiffness; for the same case with $r/\lambda = 0.6$ but with $\beta = 90^\circ$, the resulting bending stiffness is 92.61% smaller than for the square topology.

On the right side of Figure 3, bending stiffness is compared for the single and double curve topologies; the single curve topology has a larger bending stiffness than the double curve. The bending stiffness of the double curve topology is 13.12% smaller than for the single curve topology for $\beta = 90^\circ$, and 34.14% smaller for $\beta = 60^\circ$.

Yield stress is also calculated from the peak force and presented in Figure 4; on the left side, mean yield stress values for the double curve topology are plotted as a function of r/λ , and once again the yield stress is smaller as r/λ increases. For $r/\lambda = 0.6$ and $\beta = 30^\circ$, the yield stress is 70.44% smaller than for the square topology. When increasing the value of β , the yield stress decreases further; for $r/\lambda = 0.6$ and $\beta = 90^\circ$, the resulting yield stress is 94.51% smaller than for the square topology. On the right side of Figure 4, yield stress is compared between the single and double curve topologies; yield stress is also larger for this topology. The yield stress of the double curve topology is 19.54% smaller than for the single curve topology for $\beta = 30^\circ$, and 37.18% smaller for $\beta = 60^\circ$.

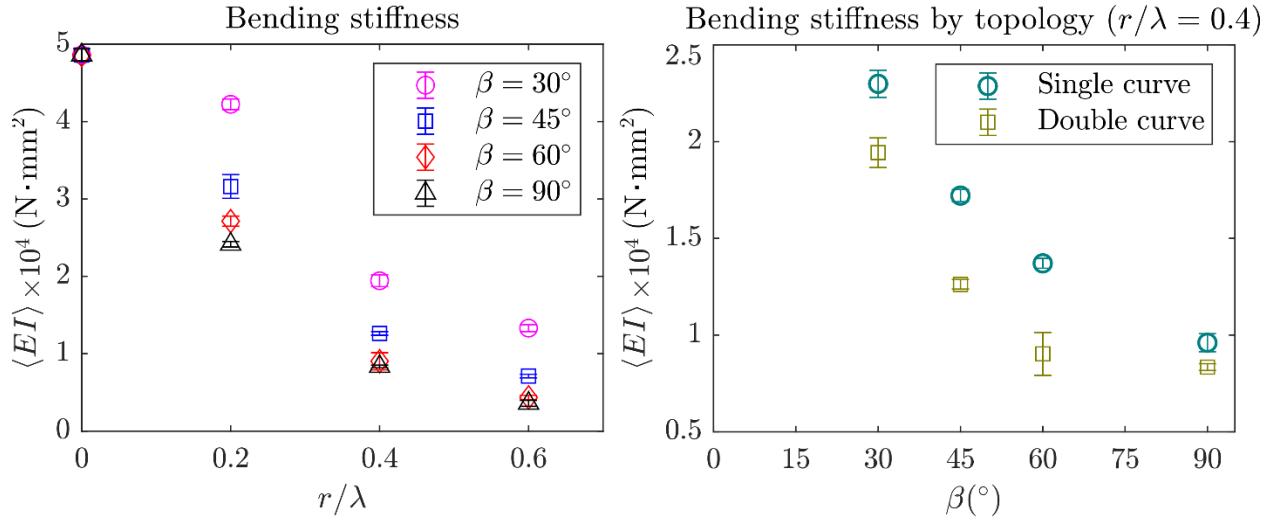


Figure 3. Left: Bending stiffness $\langle EI \rangle$ as a function of r/λ for the double curve topology; colors and markers represent different values of β . Right: Comparison of bending stiffness $\langle EI \rangle$ between single and double curve topologies (for the case with $r/\lambda = 0.4$), as a function of β . Mean values are plotted with ± 1 standard deviation error bars in all cases.

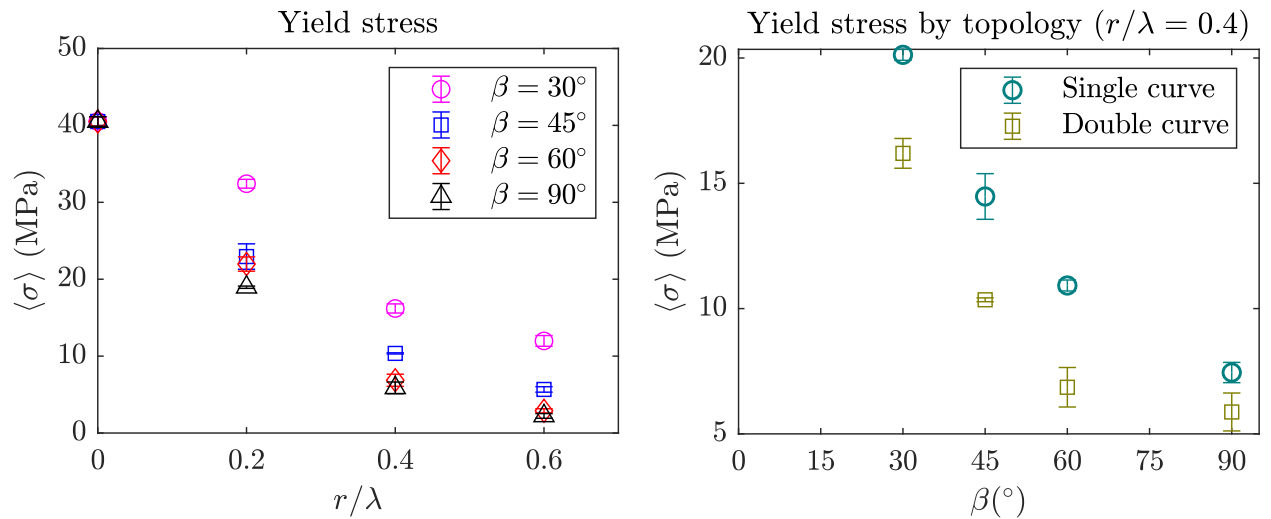


Figure 4. Left: Yield stress $\langle \sigma \rangle$ as a function of r/λ for the double curve topology; colors and markers represent different values of β . Right: Comparison of yield stress $\langle \sigma \rangle$ between single and double curve topologies (for the case with $r/\lambda = 0.4$), as a function of β . Mean values are plotted with ± 1 standard deviation error bars in all cases.

Discussion

The bending stiffness $\langle EI \rangle$ of the Bézier-based lattice beams decreases as r/λ increases. This obeys the fact that a larger distance r from the center to control point \mathbf{P}_1 results in a Bézier curve with higher curvature and arclength, leading to a higher flexibility in the arrangement, especially for the double curve topology where the bending stiffness is effectively lower. Note also that increasing β also leads to an increment of the curvature, which gives lower values of β a larger

bending stiffness. Variability among the samples is also low, which is a measure of the repeatability of the 3D printing process.

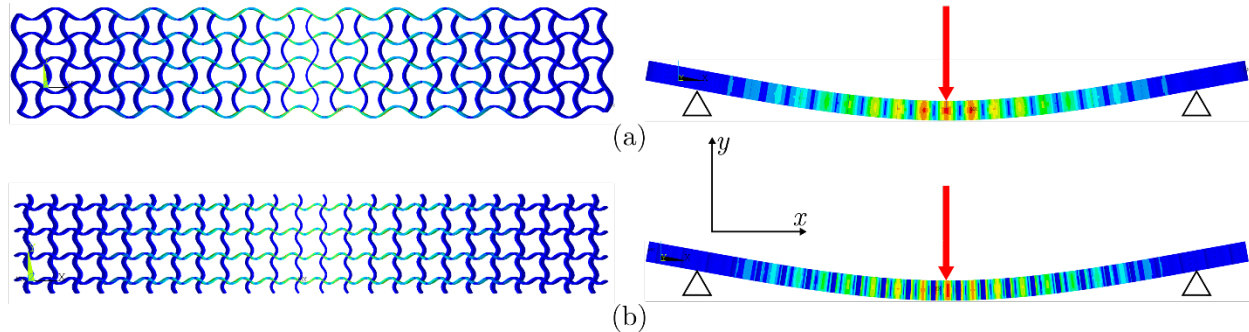


Figure 5. Qualitative finite element simulation to observe stress distribution in (a) the double curve topology and (b) the single curve topology, for $r/\lambda = 0.4$ and $\beta = 90^\circ$.

In the case of the yield stress, the force required to bend the lattice beam samples increases, since it is proportional to the bending stiffness. Considering that stress and force also have a linear relationship, stress increases with the bending stiffness. A qualitative finite element simulation of the lattice beams in bending was performed in terms of the stress distribution in the single and double lattice beam samples. Note from the simulation that in both the single and double topologies, the greatest stress concentration is in the horizontal members, which carry the load as opposed to the vertical members, which remain practically stress-free. This coincides with the loading scenario, where horizontal members effectively behave as simply supported beams in bending. However, the magnitude of the peak stress is larger in the single topology. The curvature of the Bézier curved elements has an effect on the stress distribution, since peak stresses appear at the sections of the curve with the smallest minimum radius of curvature.

Conclusions

Two topologies of Bézier-based lattice beams were fabricated and tested in three-point bending to obtain the bending stiffness and peak stress of each arrangement. The bending stiffness of lattice beams decreases when increasing the distance r between the free control point and the origin. Yield stress follows a similar behavior, and the stress concentration occurs at the horizontal members transverse to the load. When comparing the single and double curve topologies, the double curve arrangement has a larger flexibility and lower yield stress than its single curve counterpart.

The beam length and variability of the printed samples requires the characterization of deflection due to shear as future work. Other characterization methods can be used to analyze the lattice beams presented here, in order to provide a better insight on the properties of this topology and its adaptation to suit various engineering applications. Overall, the synthesis method presented here allows the design of lattice beams with custom bending stiffness and large flexibility.

Acknowledgments

This research was supported by Mexico's CONACyT Scholarship Program (1006922) for PhD studies of first author. The support of Tecnológico de Monterrey is also acknowledged.

References

- [1] K. Refai, M. Montemurro, C. Brugger, N. Saintier, Determination of the effective elastic properties of titanium lattice structures, *Mechanics of Advanced Materials and Structures* 27 (2019) 1966–1982. doi:10.1080/15376494.2018.1536816.
- [2] P. Tran, C. Peng, Triply periodic minimal surfaces sandwich structures subjected to shock impact, *Journal of Sandwich Structures and Materials* 23 (2020) 2146. doi:10.1177/1099636220905551.
- [3] I. Maskery, L. Sturm, A. O. Aremu, A. Panesar, C. B. Williams, C. J. Tuck, R. D. Wildman, I. A. Ashcroft, R. J. Hague, Insights into the mechanical properties of several triply periodic minimal surface lattice structures made by polymer additive manufacturing, *Polymer* 152 (2018) 62–71. doi:10.1016/j.polymer.2017.11.049.
- [4] D. Bhate, C. A. Penick, L. A. Ferry, C. Lee, Classification and Selection of Cellular Materials in Mechanical Design: Engineering and Biomimetic Approaches, *Designs* 3 (2019) 19. doi:10.3390/designs3010019.
- [5] L. J. Gibson, M. F. Ashby, G. S. Schajer, C. I. Robertson, The mechanics of two-dimensional cellular materials, *Proceedings of the Royal Society of London. A. Mathematical and Physical Sciences* 382 (1982) 43–59. doi:10.1098/rspa.1982.0088.
- [6] M. J. Choi, S. Cho, Isogeometric configuration design optimization of shape memory polymer curved beam structures for extremal negative Poisson's ratio, *Structural and Multidisciplinary Optimization* 58 (2018) 1861–1883. doi:10.1007/s00158-018-2088-y.
- [7] Z. P. Wang, L. H. Poh, Optimal form and size characterization of planar isotropic petal-shaped auxetics with tunable effective properties using IGA, *Composite Structures* 201 (2018) 486–502. doi:10.1016/j.compstruct.2018.06.042.
- [8] Z. P. Wang, L. H. Poh, Y. Zhu, J. Dirrenberger, S. Forest, Systematic design of tetra-petals auxetic structures with stiffness constraint, *Materials and Design* 170 (2019) 107669. doi:10.1016/j.matdes.2019.107669.
- [9] A. Álvarez-Trejo, E. Cuan-Urquizo, A. Roman-Flores, L. G. Trapaga-Martinez, J. M. Alvarado-Orozco, Bézier-based metamaterials: Synthesis, mechanics and additive manufacturing, *Materials and Design* 199 (2021) 109412. doi:10.1016/j.matdes.2020.109412.
- [10] M. Lei, W. Hong, Z. Zhao, C. Hamel, M. Chen, H. Lu, H. J. Qi, 3D Printing of Auxetic Metamaterials with Digitally Reprogrammable Shape, *ACS Applied Materials & Interfaces* 11 (2019) 22768–22776. doi:10.1021/acsami.9b06081.
- [11] L. Meng, X. Qiu, T. Gao, Z. Li, W. Zhang, An inverse approach to the accurate modelling of 3D-printed sandwich panels with lattice core using beams of variable cross-section, *Composite Structures* 247 (2020) 112363. doi:10.1016/j.compstruct.2020.112363.

- [12] Y. B. Wang, H. T. Liu, T. J. Li, Novel beam-like mechanical metamaterials with different flexural rigidities in two directions, *Composite Structures* 267 (2021) 113857. doi:10.1016/j.compstruct.2021.113857.
- [13] A. Álvarez-Trejo, A. Juárez-López, D. Zeller-Villanueva, A. Román-Flores, E. Cuan-Urquizo, Effect of shear modulus in the transverse deflection of 2D lattice beams, in: *Memorias del XXIV Congreso Internacional Anual de la SOMIM*, 2018, pp. 35–41.
- [14] V. A. Eremeyev, E. Turco, Enriched buckling for beam-lattice metamaterials, *Mechanics Research Communications* 103 (2020) 103458. doi:10.1016/j.mechrescom.2019.103458.
- [15] H. Gu, A. D. Shaw, M. Amoozgar, J. Zhang, C. Wang, M. I. Friswell, Twist morphing of a composite rotor blade using a novel metamaterial, *Composite Structures* 254 (2020) 112855. doi:10.1016/j.compstruct.2020.112855.
- [16] W. C. Young, R. G. Budynas, *Roark's formulas for stress and strain*, McGraw-Hill Education, New York, 2002.